The role of mechanical wall stress and wall shear stress on coronary artery disease

Tziotziou, Aikaterini; Fabra, Amalia de Juana; Hoogendoorn, Ayla; Korteland, Suze Anne; van der Lugt, Aad; van der Steen, Antonius F.W.; Bos, Daniel; Wentzel, Jolanda J.; Akyildiz, Ali C.

DOI
10.1016/j.cmpb.2025.108968

Publication date
2025

Document Version
Final published version

Published in
Computer Methods and Programs in Biomedicine

Citation (APA)
Tziotziou, A., Fabra, A. D. J., Hoogendoorn, A., Korteland, S. A., van der Lugt, A., van der Steen, A. F. W., Bos, D., Wentzel, J. J., & Akyildiz, A. C. (2025). The role of mechanical wall stress and wall shear stress on coronary artery disease. *Computer Methods and Programs in Biomedicine*, *270*, Article 108968. https://doi.org/10.1016/j.cmpb.2025.108968

Computer Methods and Programs in Biomedicine 270 (2025) 108968

Contents lists available at ScienceDirect

Computer Methods and Programs in Biomedicine

journal homepage: www.sciencedirect.com/journal/computer-methods-and-programs-in-biomedicine

The role of mechanical wall stress and wall shear stress on coronary artery disease

Aikaterini Tziotziou [a,b], Amalia de Juana Fabra [c], Ayla Hoogendoorn [a], Suze-Anne Korteland [a], Aad van der Lugt [b], Antonius F.W. van der Steen [a], Daniel Bos [b,d], Jolanda J. Wentzel [a], Ali C. Akyildiz [a,c,*]

[a] Department of Cardiology, Biomedical Engineering, Cardiovascular Institute, Thorax Center, Erasmus MC, Rotterdam, the Netherlands
[b] Department of Radiology & Nuclear Medicine, Erasmus Medical Center, Rotterdam, the Netherlands
[c] Department of Biomechanical Engineering, Delft University of Technology, Delft, the Netherlands
[d] Department of Epidemiology, Erasmus Medical Center, Rotterdam, the Netherlands

ARTICLE INFO

Keywords:
Atherosclerosis
Coronary artery
Wall shear stress
Mechanical wall stress
IVUS
OCT

ABSTRACT

Background and objective: Although the association of wall shear stress (WSS) with coronary artery disease has been well studied, that of mechanical wall stress (MWS) is mainly overlooked. In this study, we performed in-silico artery-specific modeling to investigate the involvement of both MWS and WSS in coronary artery disease.
Methods: Fifteen coronary arteries from five adult familial hypercholesterolemic pigs were imaged by coronary computed tomography angiography, intravascular ultrasound, and optical coherence tomography at three time points (3, 9, and 12 months). Local WSS and MWS in 3 mm/45° sectors were determined using artery-specific computational models. The relationship of WSS and MWS with wall thickness change (ΔWT) over time was statistically analyzed using Generalized Linear Mixed models.
Results: A positive ΔWT was measured in all sectors, where plaque sectors presented a greater ΔWT rate compared to plaque-free sectors. In plaque-free sectors, low WSS was associated with a higher ΔWT rate ($p < 0.001$). In plaque sectors, high MWS was associated with a higher ΔWT rate ($p < 0.05$), where ΔWT rate was, although slightly, even greater in the plaque sectors with lipid-rich necrotic core ($p < 0.05$).
Conclusions: Our results from in-silico coronary-specific models suggest that WSS and MWS may play a dominant role at different stages of coronary artery disease. WSS may be more critical in the early stages of plaque formation while MWS might have greater significance in the progression of existing plaques.

1. Introduction

Coronary artery disease involves the accumulation of atherosclerotic plaque tissue in the arterial wall, potentially causing lumen narrowing and/or blood clot formation [1–4]. The eventual consequences are the partial or complete obstruction of the artery and reduction in cardiac perfusion, which may lead to cardiac events [5–6]. Coronaries experience two primary types of biomechanical stresses; mechanical wall stress (MWS), which is induced by blood pressure, and wall shear stress (WSS), which arises from blood flow [7–8].

The flow-driven WSS derives from the friction of blood flow acting on the surface of the arterial lumen, where endothelial cells reside [9–10]. The role of WSS in coronary atherosclerosis is well researched. Endothelial cells are shown to be responsive to changes in WSS levels and can activate inflammatory pathways, which may lead to atherosclerosis [11–14]. The pressure-driven MWS, on the other hand, causes the entire arterial wall, and hence the internal microstructural components, like the vascular endothelial cells and smooth muscle cells, to stretch and expand [15–17]. MWS has been studied for its involvement in arterial remodeling under hypertensive conditions and shown to trigger extracellular matrix formation in the arterial wall [18–19]. However, its potential role in atherosclerotic plaque formation and progression has not been well studied [20–21].

While several patient studies [12,22] have provided valuable insights into coronary atherosclerosis, they often suffer from limitations such as short study duration and, a limited number of longitudinal

* Corresponding author at: Department of Cardiology, Biomedical Engineering, Cardiovascular Institute, Thorax Center, Erasmus MC, Rotterdam. Mekelweg 5, 2628 CD Delft, the Netherlands.
E-mail addresses: a.akyildiz@erasmusmc.nl, a.c.akyildiz@tudelft.nl (A.C. Akyildiz).

https://doi.org/10.1016/j.cmpb.2025.108968
Received 2 October 2024; Received in revised form 9 July 2025; Accepted 14 July 2025
Available online 14 July 2025

imaging time points [23–25]. Consequently, these studies did not cover the necessary time scales to fully research the development of atherosclerosis. Additionally, in such studies, patients are typically on medications, such as lipid-lowering statins [26–27], which alter the natural course and progression of coronary atherosclerosis. Animal models of coronary atherosclerosis can potentially address these limitations, allowing for the examination of the disease at various stages without the influence of medication [28–30].

In this study, the individual and combined effect of local WSS and MWS on coronary artery disease onset and progression was assessed. To do so, we used an animal model of adult, full-grown pigs with familial hypercholesterolemia and on an atherogenic diet. We imaged the coronary arteries of the pigs at three time points during the one-year course of the study. We created artery-specific in-silico models, to assess the local WSS and MWS in the coronary arteries of these pigs at multiple time points and to investigate their association with coronary artery disease.

2. Methods

2.1. Study design

The analysis consisted of ten castrated adult male pigs (age 34 ± 3 months) with familial hypercholesterolaemia and a mutation in the low-density lipoprotein receptor. The study focused on each pig's main coronaries (left anterior descending - LAD, left circumflex - LCX, and right coronary artery - RCA), examined at three timepoints: three (T1), nine (T2) and twelve months (T3) after initiating a high-fat diet to induce atherosclerosis (Fig. 1). The study received approval from Erasmus MC animal ethics committee and followed the National Institute of Health guidelines (Council, 2011, 109–14–10). Further details of the study are available in previous publications by our group [31–32].

2.2. Data acquisition

Coronary computed tomography angiography (CCTA) (SOMATOM Force, Siemens Healthineers, Germany), IVUS (InfraRedX, Burlington, MA, USA), and OCT (Dragonfly Optics Imaging Catheter, St Jude Medical, St Paul, MN, USA) were used to image the coronary arteries (Fig. 1). Flow velocity measurements were taken using Combowire Doppler (Volcano Corp., Rancho Cordova, CA, USA). The imaging protocol was conducted three months after starting the high-fat diet (T1) and repeated at nine months (T2) and twelve months (T3) for all pigs [31].

2.3. Wall shear stress analysis

The IVUS frames were segmented using a semi-automatic pipeline (QCU, Medis Medical Imaging, Leiden) and 3D lumen geometries at T1, T2, and T3 were reconstructed. The lumen contours at T1, T2, and T3 were also co-registered utilizing the 3D CCTA-derived centreline and the coronary side branches as landmarks (Mevislab, Bremen, Germany) [32].

Computational fluid dynamics (CFD) simulations (ANSYS Inc. Canonsburg, USA) were conducted to solve the Navier–Stokes equations on the reconstructed lumen geometries utilizing animal-specific Doppler flow measurements at T1 and T2 (Fig. 1). Blood was considered to be incompressible, non-Newtonian fluid with 1060 kg/m3 density and modelled using the Carreau model . No-slip condition was enforced, and the arterial wall was assumed to be rigid [32]. The instantaneous maximum blood flow velocity was recorded at multiple points both upstream and downstream of each side branch in every artery using the ComboWire. From the maximum velocity data, the flow rate was calculated based on the nearest proximal measurement and used as the inlet boundary condition, using a flat velocity profile with a time-dependent waveform in the CFD model. The flow ratio for each side

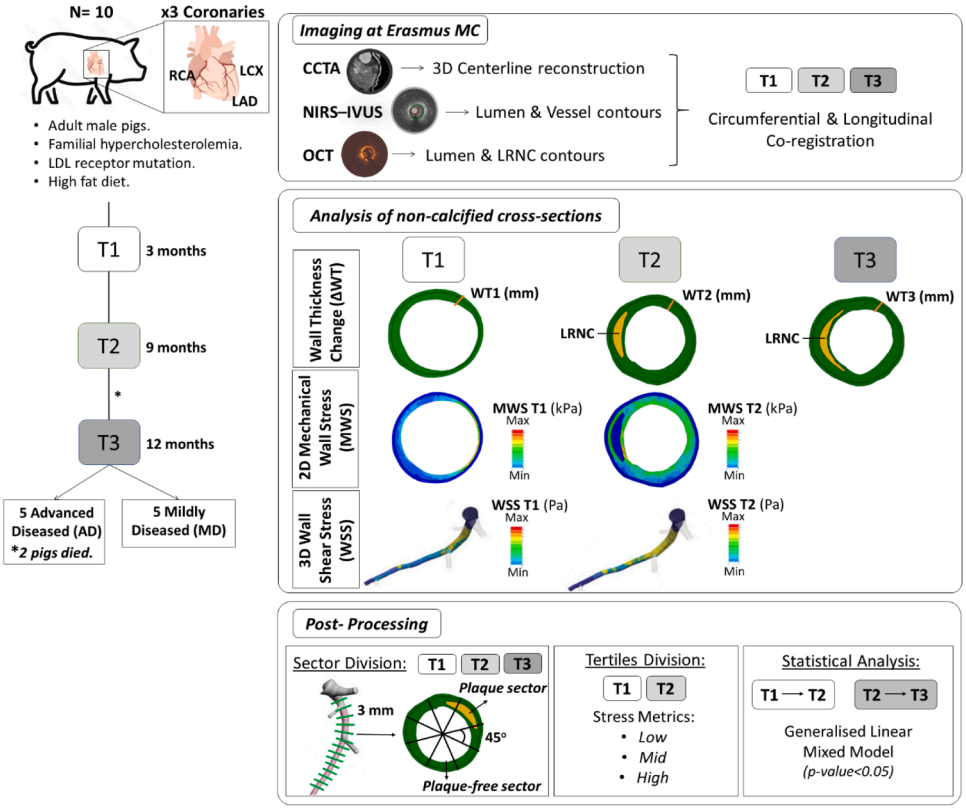

Fig. 1. Study design pipeline. (LRNC: lipid-rich necrotic core; RCA: right coronary artery; LCX: left circumflex artery; LAD: left anterior descending artery; CCTA: Coronary computed tomography angiography; NIRS-IVUS: Intravascular ultrasound - Near-infrared spectroscopy; OCT: Optical coherence tomography; MWS: mechanical wall stress; WSS: wall shear stress, and WT: wall thickness.).

branch was determined from in vivo Doppler velocity measurements by calculating the difference in flow rates between upstream and downstream velocities, and this was applied as the outflow condition [32]. In instances where the flow velocity data was either unreliable or missing, due to Doppler wire positioning, signal quality and artifacts, the Huo-Kassab diameter-based scaling law was utilized to estimate the flow ratio [32]. A comprehensive explanation of the computational fluid dynamics simulation is available in a previously published paper [32]. The time-averaged wall shear stress was calculated by averaging the shear stress readings across a heart cycle, and used throughout the text as the wall shear stress (WSS).

2.4. Mechanical wall stress analysis

The IVUS and OCT images, aligned and co-registered using an custom-built MATLAB code, were utilized to reconstruct the cross-sections every 1 mm in the coronary arteries [32]. Natural landmarks, like side branches, were utilized for precise alignment in all directions. The co-registration procedure consisted of three steps. First, a longitudinal co-registration was performed by detecting the position of the side-branches of each artery (reference frames) in both IVUS and OCT images. Second, a circumferential co-registration was done by rotating the reference OCT frames so that they were aligned to the corresponding reference IVUS frame. Lastly, a linear interpolation of matching and rotations was done between the reference frames so that all OCT frames would match IVUS frame. IVUS frames were used to segment the external elastic lamina (EEL), depicting the artery's exterior wall. A consistent (0.15 mm) layer was included to account for the adventitia layer's stiffness [15]. Regions containing calcifications, which hindered the segmentation of the EEL, were excluded from the analysis. To ensure consistency in our study, we excluded all cross-sections with calcifications, regardless of their size, in the analyses from T1 to T2 (31 cross-sections, 7.4 %) and from T2 to T3 (49 cross-sections, 16 %). Side-branch locations were also excluded due to their incomplete circumferential structural integrity in the analyses from T1 to T2 (19 cross-sections, 4.5 %) and from T2 to T3 (11 cross-sections, 3.6 %). The outer borders of the lipid-rich necrotic core (LRNC) contours were reconstructed based on an in-house MATLAB algorithm [33].

At T1 and T2, mechanical wall stress (MWS) was calculated using a Finite Element Analysis (FEA) technique (Fig. 1) in ABAQUS (2019, Dassault Systèmes). First, the 2D cross-sectional geometries were imported into the FE modeling software ABAQUS including the lumen, outer vessel wall and LRNC contours. Eventually, the FE models contained intima/media component, adventitia component, and if present, LRNC. The material properties were modeled as isotropic, nonlinear, hyperelastic, and incompressible, using a modified Mooney-Rivlin model for the intima/media, a Yeoh model for the adventitia, and a Neo-Hookean model for the LRNC components [7,15–16] (Supplementary Data). The backward incremental approach [15] was utilised to ascertain the existing stresses within the coronary geometries. The FEA was completed using plane strain assumption and patient-specific blood pressure readings. A mesh convergence evaluation was conducted, and each cross-section consisted of ~11,000 elements of the CPE4H type (4-node hybrid, linear plane strain triangle). The FE simulations outputted the von Mises MWS. This manuscript reports both the maximum luminal MWS (i.e., the maximum of the MWS at the lumen nodes) and the average MWS within the artery (i.e., the average of the MWS of the vessel wall nodes).

2.5. Vessel wall growth

The vessel wall growth was determined by the vessel wall thickness change over time (ΔWT). At T1, T2, and T3, the intima and media width—radial length between lumen and the external elastic lamina—was measured in order to calculate the wall thickness (WT) (Fig. 1). The lipid-rich necrotic core (LRNC) presence in a segment was determined based on the OCT frames assessment [31]. Specifically, a segment was labeled as LRNC segment when at least 50 % of it was identified as lipid-rich on the OCT frames [34].

2.6. Statistical analysis

Every artery was separated into sectors that were 3 mm long (longitudinally) and 45° wide (circumferentially) (Fig. 1) to ensure maximum overlap of the T1, T2, and T3 data while accounting for spatial heterogeneity. The sectors were split, based on 0.5 mm thickness, into sectors free of plaque or plaque-containing [31], as illustrated in Fig. 1. The assessments for the sectors with and without plaque were conducted independently at T1, T2, and T3, to research disease development and evolution. At T1 and T2, the WSS and MWS values for each sector type were separated into low, mid, and high tertiles.

Spearman correlation was employed to assess the level of correlation between WSS and MWS at T1 and T2. To investigate the association of stress metrics with vessel wall changes over time, the Generalized Linear Mixed Model (GLMM) with gamma regression distribution and log link transformation was utilized, as the residuals of the linear mixed model were not normally distributed. In the statistical analysis at T1, the sector-level stress metrics at T1 (i.e., WSS tertiles and MWS tertiles) were correlated with WT at T2, adjusted for WT at T1 and the average cholesterol level at T1. The ΔWT from T1 to T2 was calculated by subtracting the adjusted WT at T1 from the estimated WT at T2 and then normalized for the number of months between T1 and T2, resulting in a measure of ΔWT rate (mm/month). The same procedure was applied for the analysis from T2 to T3. Stress metrics and their interaction were included as fixed factors. Repeated comparisons of the p-values were corrected using the Bonferroni technique. A two-tailed $p < 0.05$ was chosen as the significance level, using SPSS (IBM 27). The artery and animal information were treated as random factors to account for the intra-artery and intra-animal dependencies in the sector-level data.

3. Results

Five of the 10 pigs had to be excluded from any further analysis due to limited plaque development from T1 to T3 (mean plaque burden of 16 % [10 %–20 %] at T3). Specifically, 82 % of their sectors were still plaque-free after one year follow-up with minimum or no wall thickness change over time. There were no significant differences in housing conditions, diet, seasonal period, or birth year between these five pigs and the rest of the pigs that developed atherosclerosis. However, a distinct variation in the low-density lipoprotein profile of the five pigs that developed advanced atherosclerosis may help explain these differences [31–32,35]. Intrigued by this unexpected finding, our group performed an extensive lipoprotein analysis and found out a distinct LDL-profile with 'regular' and 'larger' LDL. In this distinct LDL profile, the distribution of cholesterol and sphingolipids over both LDL subclasses was directly related to the eventual atherosclerotic disease severity in the pigs. Hence, all subsequent results are based on the remaining five pigs, which developed significant, lumen-intruding plaques in the coronary arteries from T1 to T3, with a mean plaque burden of 30 % [18 %–49 %] at T3. Traditional cardiovascular risk factors remained stable over time for the five pigs studied (Table S1, Supplementary Data). Two of the five pigs passed away from myocardial infarction during T2 -T3 and only the study from T1 to T2 included data from these pigs.

The Spearman test for T1 and T2 indicated no correlation of WSS with luminal MWS or within-vessel MWS ($r < 0.20$). MWS at lumen and arterial wall exhibited comparable stress outcomes and a strong association ($r > 0.70$) (Table S2, Supplementary Data). Thus, in subsequent statistical studies, WSS and MWS at the lumen were included. Luminal MWS was chosen over within-vessel MWS because the reports from the previous research on plaque remodeling, progression, and vulnerability have mainly concentrated on the luminal region [7,17,19].

3.1. Biomechanics at T1 and wall thickness change from T1 to T2

From the 15 coronary arteries (5 LADs, 5 RCAs, and 5 LCXs) from the five pigs imaged at T1 and T2, a total of 2952 sectors were analyzed. At T1, almost all (98 %, $n = 2906$) of these sectors were free of plaque, with median WT of 0.17 mm [0.08–0.24 mm] (Table S3-S4, Supplementary Data) and 541 (18 %) of these sectors were identified as plaque at T2.

3.1.1. Plaque – free sectors at T1

During six-month period from T1 to T2, plaque-free sectors exhibited a mean ΔWT rate of 0.03 mm/month, with 83 % presenting vessel wall growth. For WSS, the tertiles were separated based on 0.62 Pa and 0.96 Pa and for MWS tertiles, the 279 kPa and 466 kPa values were used. Statistical analyses using GLMM revealed a significant negative association between WSS at T1 and ΔWT rate (T1 to T2) ($p < 0.001$). Lower levels of WSS at T1 were associated with higher mean ΔWT rate (T1 to T2) (Fig. 2A). MWS showed no association with ΔWT rate (T1 to T2) ($p = 0.66$) (Fig. 2B) (Table S5, Supplementary Data).

3.2. Biomechanics at T2 and wall thickness change from T2 to T3

The three pigs that survived until T3 provided the nine coronary arteries (3 LADs, 3 RCAs, and 3 LCXs), which were imaged at T3. Of the 1955 sectors analyzed from these arteries, 80 % ($n = 1555$) were plaque-free at T2 while the remaining 20 % ($n = 400$) were plaque sectors. At T3, 607 (31 %) sectors were plaque-containing. The median WT at T2 for the plaque-free sectors was 0.23 mm [0.12–0.32 mm] whereas for the plaque sectors, it was 0.61 mm [0.54–0.75 mm] (Table S3-S4, Supplementary Data).

3.2.1. Plaque – free sectors at T2

During the three-month follow-up, plaque-free sectors exhibited a mean ΔWT rate of 0.03 mm/month, and 69 % of these sectors showed a gradual increase in thickness. For WSS, the tertiles were separated based on 0.45 Pa and 0.74 Pa and for MWS tertiles, the 152 kPa and 265 kPa values were used. The results of the GLMM statistical analysis presented a significant negative association between WSS at T2 and ΔWT rate (T2 to T3) ($p < 0.001$) in the plaque-free sectors (Fig. 3A) and MWS was not associated with ΔWT rate (T2 to T3) ($p = 0.35$) (Fig. 3B) (Table S6, Supplementary Data).

3.2.2. Plaque sectors at T2

Over the course of three months between T2 and T3, plaque sectors ($n = 400$) exhibited an average ΔWT rate of 0.05 mm/month, and 58 % of these sectors demonstrated an increase in thickness over time. For WSS, the tertiles were separated based on 0.55 Pa and 0.97 Pa and for MWS tertiles, the 56 kPa and 122 kPa values were used. Interestingly, the statistical analysis could not demonstrate any significant association of WSS with ΔWT rate ($p = 0.21$) (Fig. 4A). However, a significant positive correlation was observed between MWS and ΔWT rate ($p = 0.003$). Sectors with higher levels of MWS exhibited a higher mean ΔWT rate (Fig. 4B) (Table S6, Supplementary Data).

Plaque sectors at T2 were further stratified based on the presence of LRNC at T2. At T2, 34 % ($n = 137$) of the plaque sectors were labeled as LRNC sectors, and these sectors had a mean ΔWT rate of 0.04 mm/month (Table S6, Supplementary Data). Both sectors with and without LRNC confirmed a positive association of MWS at T2 with ΔWT rate (T2 to T3) (Fig. 5), where the LRNC sectors had slightly higher ΔWT rates than their LRNC-free counterparts.

4. Discussion

In this study, we examined the influence of the individual and combined effect of MWS and WSS on the development of coronary artery disease, using an adult familial hypercholesterolemia pig model with advanced atherosclerosis. The main findings of our study are as follows: (1) coronary plaque sectors present a greater ΔWT rate compared to plaque-free sectors, (2) low WSS is associated with greater vessel wall growth at plaque-free sectors, (3) high MWS is associated with greater wall thickness increase at plaque sectors, and (4) regions with LRNC subjected to high MWS show greater wall thickness increase.

The measurements at T1 showed that the majority of the arterial sectors were still plaque-free, although the pigs had been on an atherogenic diet already for 3 months. However, by T2 (9 months on the atherogenic diet) and T3 (12 months on the atherogenic diet), lumen intruding plaques were present, reflecting the initiation and growth of atherosclerosis. Overall, over the complete one-year follow-up time of the study, there was an increase in wall thickness in all sectors, even in the ones that were still categorized as plaque-free at T3 and, in a small percentage of sectors, LRNC structures were formed. Our results revealed that plaque sectors presented a greater ΔWT rate compared to plaque-free sectors. Regions with atherosclerotic plaques tend to grow faster and more extensively compared to plaque-free regions in arteries,

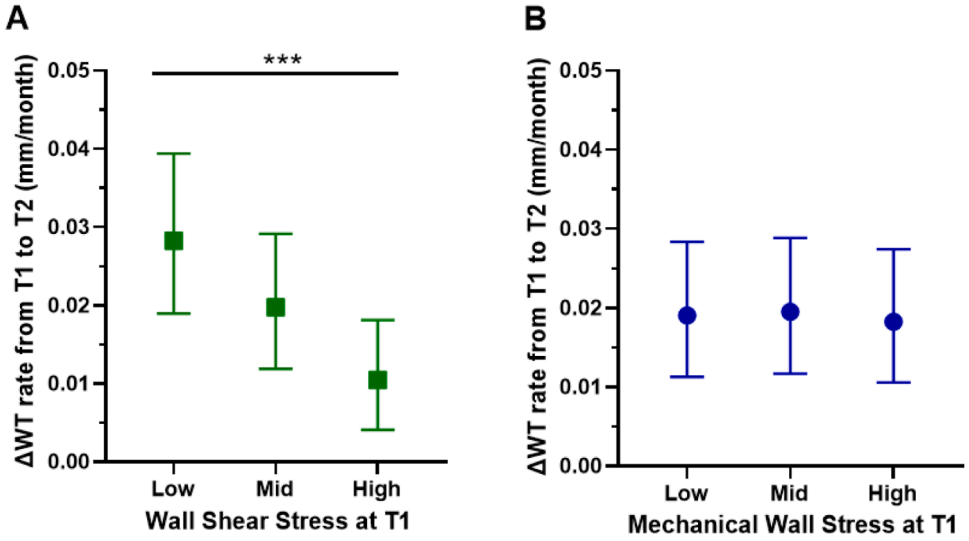

Fig. 2. Plaque-free sectors at T1: (A) Association of WSS at T1 with ΔWT rate between T1 and T2 (B) Association of MWS at T1 with ΔWT rate between T1 and T2, based on Generalized Linear Mixed Model. (Data are presented as mean with 95 % CI: Confidence Interval; ΔWT rate: wall thickness change per month; ***: $p < 0.001$).

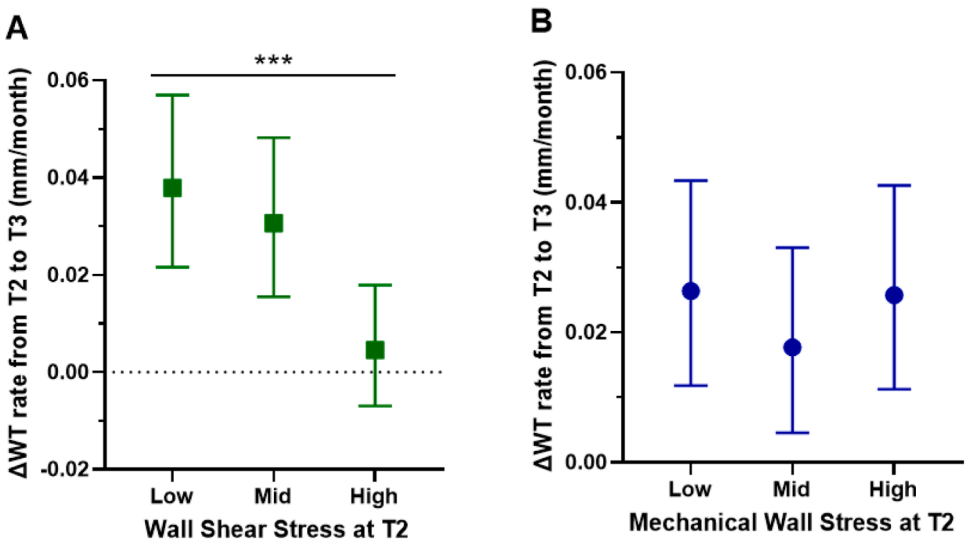

Fig. 3. Plaque-free sectors at T2: (A) Association of WSS at T2 with ΔWT rate between T2 and T3 (B) Association of MWS at T2 with ΔWT rate between T2 and T3, based on Generalized Linear Mixed Model. (Data are presented as mean with 95 % CI: Confidence Interval; ΔWT rate: wall thickness change per month; ***: $p < 0.001$).

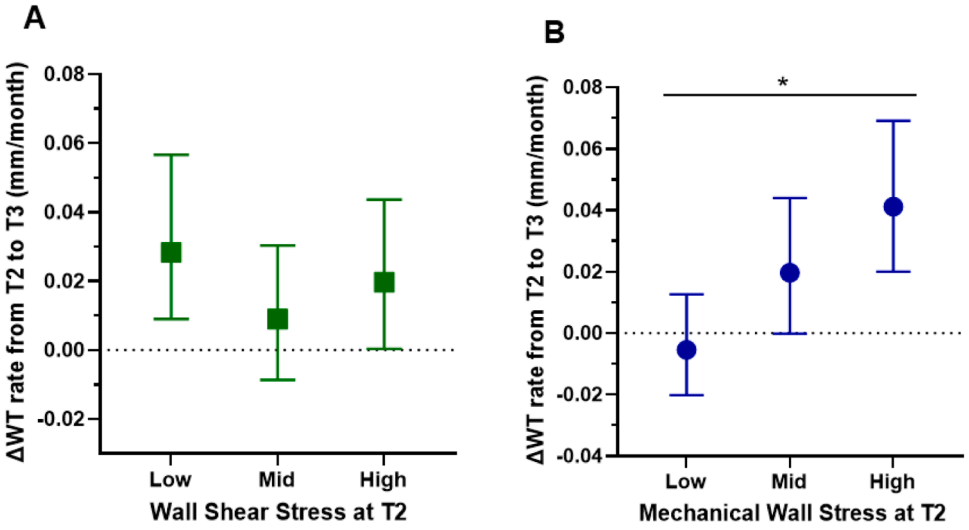

Fig. 4. Plaque sectors at T2: (A) Association of WSS at T2 with ΔWT rate between T2 and T3 (B) Association of MWS at T2 with ΔWT rate between T2 and T3, based on Generalized Linear Mixed Model. (Data are presented as mean with 95 % CI: Confidence Interval; ΔWT rate: wall thickness change per month; *: $p < 0.05$).

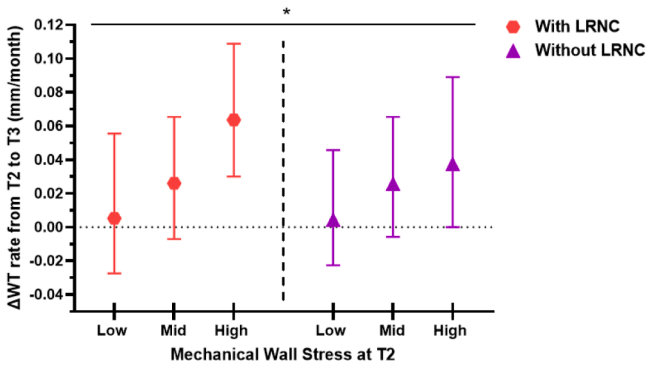

Fig. 5. Plaque sectors at T2: Association of MWS at T2 with ΔWT rate between T2 and T3, stratified by LRNC presence, based on Generalized Linear Mixed Model. (Data are presented as mean with 95 % CI: Confidence Interval; ΔWT rate: wall thickness change per month; LRNC: lipid-rich necrotic core; *: $p < 0.05$).

implying an increasing rate in the course of atherosclerosis. This can be explained by the ongoing inflammation, lipid accumulation, and tissue remodeling, possibly accelerating the growth of these plaques [36]. Specifically, compared to plaque-free sectors, in plaque sectors the endothelium is already dysfunctional allowing more lipoproteins and inflammatory cells to enter the arterial wall, promoting faster plaque development [36]. The differing growth rates between plaque and plaque-free sectors could potentially enable more targeted monitoring of areas with existing plaque, support personalized treatment strategies, and enhance current risk assessment models.

Our analyses of plaque-free sectors provided insights into the involvement of biomechanical factors in the natural history of atherosclerosis initiation. For plaque-free sectors (identified at T1 and T2), WSS was negatively associated with ΔWT rate, where low WSS was associated with the greatest increase in wall thickness over time. This finding aligns well with earlier studies [37–38] that investigated atherosclerosis in pig models. The atherogenic mechanotransductive mechanisms, such as low WSS activating athero-inflammatory pathways

(e.g., NF-kB pathway), by affecting the alignment and organization of the endothelial cells have been reported before [39]. This finding suggests that low WSS could serve as a valuable metric for the early identification of high-risk areas, aiding in the prediction and prevention of atherosclerotic plaque development, and contributing to personalized risk models to support more informed clinical decision-making. The other biomechanical factor, the MWS, did not correlate with the ΔWT rate for plaque-free sectors, which may imply that MWS is not a primary biomechanical factor in atherosclerosis initiation.

Our analyses on plaque sectors, to understand the influence of biomechanical factors in the natural history of atherosclerosis plaque progression, could not show any significant association of WSS at plaque sectors with ΔWT rate. Previous analyses of our dataset [32,40] presented a significant negative association of WSS and ΔWT rate, but without a separate analysis for plaque-free and plaque sectors. We found a strong correlation between MWS and ΔWT rate, where the sectors with high MWS demonstrated the greatest increase in wall thickness. Moreover, the highest ΔWT rate occurred in plaque sectors with existing LRNC under high MWS. So far the potential involvement of MWS in atherosclerosis has been overlooked, although in-vitro studies suggested atherogenic mechanisms being triggered by the endothelial cells, located on the lumen, and smooth muscle cells, located deeper in the arterial wall, when exposed to elevated MWS (or wall stretch) [41]. Specifically, uniaxial [42–43] and biaxial [44] stretching of endothelial cells have been reported to enhance inflammatory responses via the NF-κB-COX pathway. High MWS, potentially caused by hypertension, was shown to stimulate smooth muscle cells for increased extracellular matrix synthesis [21,45]. Unfortunately, luminal MWS and MWS in the vessel wall in our study were highly correlated, which prevents us from suggesting which specific biomechanical mechanisms and pathways are involved in plaque progression.

Overall, our study on advanced-diseased pigs demonstrated a strong association of WSS with ΔWT rate for plaque-free sectors and a strong association of MWS with ΔWT rate for plaque sectors. This finding may suggest that different biomechanical factors have a dominant role at different stages of atherosclerosis. Specifically, WSS may play a (more) important role in plaque initiation whereas MWS may be (more) important for plaque progression.

Comparing our results with previously published studies on human coronaries [11–13,46], WSS at plaque-free sectors followed the same negative association with ΔWT over time, presenting the known association between low WSS and atherosclerotic plaque initiation. In contrast to the existing literature on human coronaries [11–12], our study revealed no significant association at plaque sectors between WSS and ΔWT rate, which may be due to the short interval of 3 months between T2 and T3.

Concerning the analysis of MWS in our study, to the best of our knowledge, our study is the first natural history study of coronary artery disease focusing on the association of MWS with the disease. Contrary to our previously published study on human coronaries [46], MWS in plaque-free sectors in the studied pigs presented no significant association with ΔWT rate. Moreover, at plaque sectors, the MWS was positively correlated with wall thickness increase over time, opposite to the finding in previous human coronary atherosclerosis studies [7,46]. One must note that patients involved in the human atherosclerosis studies are on statin therapy, which is well-known for its effectiveness in slowing, if not reversing, the progression of atherosclerosis [47–48].

In the current study, we employed an animal model of advanced atherosclerosis, which allowed us to study the natural course of the disease, with no therapy or medication effects involved. Animal models that closely reflect human atherosclerosis disease are necessary in order to increase the translational relevance to patient studies and to more accurately represent the course of human atherosclerosis over time. Furthermore, several follow-up time periods can be useful to document the onset and progression of atherosclerosis. Human research and animal models complement each other, and human-mimicking animal models may offer a platform for testing novel treatments and imaging methods.

Such animal models are of great use for atherosclerosis research and are commonly employed both for experimental and computational studies, where the reliability of hemodynamics in these atherosclerosis models to human atherosclerosis disease were demonstrated [35]. Our findings strongly suggest a pivotal role of local biomechanics in atherosclerosis, which may encourage biomechanical analyses for multidisciplinary atherosclerosis research and clinical practice in the future. Despite the current labour-intensive methods and long computational times that are still needed for WSS and MWS calculation, complicating direct assistance during invasive procedures, a deeper understanding of localized biomechanical effects and their spatial distribution could offer valuable insights into vascular remodeling in coronary arteries and support the development of improved and personalized strategies for patient risk-assessment and prevention or early detection of ischemic events based on biomechanical analysis in coronary arteries.

There are some limitations to consider in this study. First, five of the ten pigs had to be excluded from the analysis due to their unexpectedly limited atherosclerosis progression, leading to a small number of arteries with advanced plaque development to be analyzed. Yet, our strategy of including multiple sectors within a single coronary artery for local assessment, while accounting for the intra-artery and intra-animal dependencies, allowed us to show some statistically significant associations. Second, large calcifications, greater than 90°, obstructed the visualization of the external elastic lamina and complicated the reconstruction of the computational models. To maintain consistency, we excluded all cross-sections with calcifications and our study is confined to non-calcified cross-sections. Third, the examination of arterial segments at the side branches was not possible because the 2D FE models required the circumference to be complete. Lastly, rigid wall and static cardiac motion conditions [34] were used in the CFD analysis, which have been demonstrated to have negligible effect on the time-averaged stress measures [49].

5. Conclusion

In-silico models are of great importance for understanding and treatment management of coronary artery disease. In this study, by employing artery-specific in-silico models, we examined the individual and combined effect of the biomechanical factors (i.e., wall shear stress and mechanical wall stress) a coronary artery experiences on the onset and progression of atherosclerosis in natural history setting, utilizing a pig model in advanced stage of atherosclerotic disease. We observed the low wall shear stress to be associated with greater local wall thickness increase in plaque-free coronary sectors. For the sectors with already-existing plaque, high mechanical wall stress was associated with greater wall growth, where the sectors with lipid rich necrotic cores were, although slightly, under even greater influence of mechanical wall stress. Our findings provide new insights into the coronary artery disease and the involvement of the biomechanical factors in the pathology.

Ethics statement

This study was reviewed and approved by the DEC: Dier Experimentele Commissie (EMC nr 109-14-10). The study also received approval from Erasmus MC animal ethics committee (EMC nr. 109-14-10) and followed the National Institute of Health guidelines for the care and use of laboratory animals (Council, 2011).

Compliance with ethical standards

This study was reviewed and approved by DEC: Dier Experimentele Commissie (EMC nr 109–14–10).

Funding

This research is part of a project that has received funding from the European Research Council (ERC) under Horizon 2020 research and innovation program (Grant agreement No. 101042724 — MicroMechAthero).

Aikaterini Tziotziou was supported by Erasmus MC MRace grant PhD project.

CRediT authorship contribution statement

Aikaterini Tziotziou: Writing – original draft, Visualization, Validation, Software, Methodology, Investigation, Formal analysis, Data curation, Conceptualization. **Amalia de Juana Fabra:** Writing – review & editing, Data curation. **Ayla Hoogendoorn:** Writing – review & editing, Data curation. **Suze-Anne Korteland:** Writing – review & editing, Software, Data curation. **Aad van der Lugt:** Writing – review & editing, Supervision. **Antonius F.W. van der Steen:** Supervision, Writing – review & editing. **Daniel Bos:** Writing – review & editing, Supervision. **Jolanda J. Wentzel:** Conceptualization, Writing – review & editing. **Ali C. Akyildiz:** Supervision, Conceptualization, Writing – review & editing.

Declaration of competing interest

The authors declare that they have no known competing financial interests or personal relationships that could have appeared to influence the work reported in this paper.

Data availability statement

The data will be made available from the corresponding author upon reasonable request.

Supplementary materials

Supplementary material associated with this article can be found, in the online version, at doi:10.1016/j.cmpb.2025.108968.

References

[1] C.D. Mathers, D. Loncar, Projections of global mortality and burden of disease from 2002 to 2030, PLoS. Med. 3 (2006) 442.
[2] S.S. Virani, A. Alonso, H.J. Aparicio, et al., Heart Disease and Stroke statistics-2021 update: a report from the American Heart Association, Circulation 254 (143) (2021) 743, https://doi.org/10.1161/CIR.0000000000000950.
[3] B.R. Kwak, M. Bäck, M.L. Bochaton-Piallat, et al., Biomechanical factors in atherosclerosis: mechanisms and clinical implications, Eur. Heart. J. 35 (43) (2014) 3013–3020.
[4] U. Morbiducci, A.M. Kok, B.R. Kwak, et al., Atherosclerosis at arterial bifurcations: evidence for the role of haemodynamics and geometry, Thromb. Haemostasis 115 (3) (2016) 484–492.
[5] A. Farb, A.L. Tang, A.P. Burke, et al., Sudden coronary death. Frequency of active coronary lesions, inactive coronary lesions, and myocardial infarction, Circulation (92) (1995) 1701–1709, https://doi.org/10.1161/01.cir.92.7.1701.
[6] F.D. Kolodgie, A.P. Burke, A. Farb, et al., The thin-cap fibroatheroma: a type of vulnerable plaque: the major precursor lesion to acute coronary syndromes, Curr. Opin. Cardiol. (16) (2001) 285–292.
[7] C. Costopoulos, L.H. Timmins, Y. Huang, et al., Impact of combined plaque structural stress and wall shear stress on coronary plaque progression, regression, and changes in composition, Eur. Heart. J. (40) (2019) 1411–1422, https://doi.org/10.1093/eurheartj/ehz132.
[8] D.E. Conway, M.A. Schwartz, Flow-dependent cellular mechanotransduction in atherosclerosis, J. Cell Sci. (126) (2013) 5101–5109, https://doi.org/10.1242/jcs.138313.
[9] Y.S. Chatzizisis, M. Jonas, A.U. Coskun, et al., Prediction of the localization of high-risk coronary atherosclerotic plaques on the basis of low endothelial shear stress-an intravascular ultrasound and histopathology natural history study, Circulation (117) (2008) 993–1002.
[10] K.C. Koskinas, Y.S. Chatzizisis, M.I. Papafaklis, et al., Synergistic effect of local endothelial shear stress and systemic hypercholesterolemia on coronary atherosclerotic plaque progression and composition in pigs, Int. J. Cardiol. (169) (2013) 394–401.
[11] J.J. Wentzel, Y.S. Chatzizisis, F.J.H. Gijsen, et al., Endothelial shear stress in the evolution of coronary atherosclerotic plaque and vascular remodelling: current understanding and remaining questions, Cardiovasc. Res. (96) (2012) 234–243.
[12] P.H. Stone, S. Saito, S. Takahashi, et al., Prediction of progression of coronary artery disease and clinical outcomes using vascular profiling of endothelial shear stress and arterial plaque characteristics: the PREDICTION Study, Circulation (126) (2012) 172–181.
[13] P.H. Stone, A. Maehara, A.U. Coskun, et al., Role of low endothelial shear stress and plaque characteristics in the prediction of nonculprit major adverse cardiac events: the PROSPECT study, JACC. Cardiovasc. ImAging (11) (2018) 462–471.
[14] H. Samady, P. Eshtehardi, M.C. McDaniel, et al., Coronary artery wall shear stress is associated with progression and transformation of atherosclerotic plaque and arterial remodeling in patients with coronary artery disease/clinical perspective, Circulation (124) (2011) 779–788.
[15] A.C. Akyildiz, L. Speelman, H.A. Nieuwstadt, et al., The effects of plaque morphology and material properties on peak cap stress in human coronary arteries, Comput. Methods Biomech. Biomed. Eng. (19) (2016) 771–779, https://doi.org/10.1080/10255842.2015.1062091.
[16] A.C. Akyildiz, L. Speelman, H. van Brummelen, et al., Effects of intima stiffness and plaque morphology on peak cap stress, Biomed. Eng. Online (10) (2011) 25, https://doi.org/10.1186/1475- 925X-10-25.
[17] A.J. Brown, Z. Teng, P.C. Evans, et al., Role of biomechanical forces in the natural history of coronary atherosclerosis, Nat. Rev. Cardiol. (13) (2016) 210–220, https://doi.org/10.1038/nrcardio.2015.203.
[18] J. Ohayon, G. Finet, A.M. Gharib, et al., Necrotic core thickness and positive arterial remodeling index: emergent biomechanical factors for evaluating the risk of plaque rupture, Am. J. Physiol. Heart. Circ. Physiol. (295) (2008) 717–727, https://doi.org/10.1152/ajpheart.00005.2008.
[19] J.D. Humphrey, D.G. Harrison, C.A. Figueroa, et al., Central artery stiffness in hypertension and aging, Circ. Res. (118) (2016) 379–381, https://doi.org/10.1161/CIRCRESAHA.115.307722.
[20] G.C. Cheng, H.M. Loree, R.D. Kamm, et al., Distribution of circumferential stress in ruptured and stable atherosclerotic lesions. A structural analysis with histopathological correlation, Circulation (87) (1993) 1179–1187, https://doi.org/10.1161/01.CIR.87.4.1179.
[21] D. Tang, Z. Teng, G. Canton, et al., Sites of rupture in human atherosclerotic carotid plaques are associated with high structural stresses: an in vivo MRI-based 3D fluid-structure interaction study, Stroke (40) (2009) 3258–3263, https://doi.org/10.1161/STROKEAHA.109.558676.
[22] J.M. Cheng, H.M. Garcia-Garcia, S.P.M. de Boer, et al., In vivo detection of high-risk coronary plaques by radiofrequency intravascular ultrasound and cardiovascular outcome: results of the ATHEROREMO-IVUS study, Eur. Heart. J. (35) (2014) 639–647, https://doi.org/10.1093/eurheartj/eht484.
[23] A. Daugherty, A.R. Tall, M.J.A.P. Daemen, et al., Recommendation on design, execution, and reporting of Animal Atherosclerosis studies: a scientific statement from the American Heart Association, Arterioscler. Thromb. Vasc. Biol. (37) (2017) 131–157, https://doi.org/10.1161/ATV.0000000000000062.
[24] A. Millon, E. Canet-Soulas, L. Bousse, et al., Animal models of atherosclerosis and magnetic resonance imaging for monitoring plaque progression, Vascular. (22) (2014) 221–237, https://doi.org/10.1177/1708538113478758.
[25] L. Xiangdong, L. Yuanwu, Z. Hua, et al., Animal Models for the atherosclerosis research: a review, Protein Cell (2) (2011) 189–201, https://doi.org/10.1007/s13238-011-1016-3.
[26] S. Lee, H. Chang, J. Sung, et al., Effects of statins on coronary atherosclerotic plaques, J. Am. Coll. Cardiol. Img. (11) (2018) 1475–1484, https://doi.org/10.1016/j.jcmg.2018.04.015.
[27] M.A. Shuhaili, I.N. Samsudin, J. Stanslas, et al., Effects of different types of statins on lipid profile: a perspective on Asians, Int. J. Endocrinol. Metab. (22) (2017) 43319, https://doi.org/10.5812/ijem.43319.
[28] G.S. Getz, C.A. Reardon, Animal models of atherosclerosis, Arterioscler. Thromb. Vasc. Biol. (32) (2012) 1104–1115, https://doi.org/10.1161/ATVBAHA.111.237693.
[29] D. Hamamdzic, R.L. Wilensky, Porcine models of accelerated coronary atherosclerosis: role of diabetes mellitus and hypercholesterolemia, J. Diabetes. Res. (2013) 761415, https://doi.org/10.1155/2013/761415.
[30] T. Thim, M.K. Hagensen, L. Drouet, et al., Familial hypercholesterolaemic downsized pig with human-like coronary atherosclerosis: a model for preclinical studies, EuroIntervention. (6) (2010) 261–268.
[31] A. Hoogendoorn, S. den Hoedt, E.M.J. Hartman, et al., Variation in coronary atherosclerosis severity related to a distinct LDL (Low-Density Lipoprotein) profile: findings from a familial hypercholesterolemia pig model, Arterioscler. Thromb. Vasc. Biol. 39 (11) (2019) 2338–2352, https://doi.org/10.1161/ATVBAHA.119.313246.
[32] A. Hoogendoorn, A.M. Kok, E.M.J. Hartman, et al., Multidirectional wall shear stress promotes advanced coronary plaque development: comparing five shear stress metrics, Cardiovasc. Res. 116 (6) (2020) 1136–1146, https://doi.org/10.1093/cvr/cvz212.
[33] A.M. Kok, L. Speelman, R. Virmani, et al., Peak cap stress calculations in coronary atherosclerotic plaques with an incomplete necrotic core geometry, Biomed. Eng. Online (15) (2016) 48, https://doi.org/10.1186/s12938-016-0162-5.
[34] E.M.J. Hartman, G. De Nisco, A.M. Kok, et al., Wall shear stress-related plaque growth of lipid-rich plaques in human coronary arteries: an near-infrared spectroscopy and optical coherence tomography study, Cardiovasc. Res. 119 (4) (2023) 1021–1029, https://doi.org/10.1093/cvr/cvac178.
[35] G. De Nisco, C. Chiastra, E.M.J. Hartman, et al., Comparison of swine and Human computational hemodynamics models for the study of coronary atherosclerosis,

Front. Bioeng. Biotechnol. 9 (2021) 731924, https://doi.org/10.3389/fbioe.2021.731924.
[36] M.A. Gimbrone Jr, G. García-Cardeña, Endothelial cell dysfunction and the pathobiology of atherosclerosis, Circ. Res. 118 (4) (2016) 620–636, https://doi.org/10.1161/CIRCRESAHA.115.306301.
[37] V. Mazzi, G. De Nisco, A. Hoogendoorn, et al., Early atherosclerotic changes in coronary arteries are associated with endothelium shear stress contraction/expansion variability, Ann. Biomed. Eng. 49 (9) (2021) 2606–2621, https://doi.org/10.1007/s10439-021-02829-5.
[38] K.C. Koskinas, C.L. Feldman, Y.S. Chatzizisis, et al., Natural history of experimental coronary atherosclerosis and vascular remodeling in relation to endothelial shear stress: a serial, in vivo intravascular ultrasound study, Circulation 121 (19) (2010) 2092–2101, https://doi.org/10.1161/CIRCULATIONAHA.109.901678.
[39] Y.S. Chatzizisis, A.U. Coskun, M. Jonas, et al., Role of endothelial shear stress in the natural history of coronary atherosclerosis and vascular remodeling: molecular, cellular, and vascular behavior, J. Am. Coll. Cardiol. 49 (25) (2007) 2379–2393, https://doi.org/10.1016/j.jacc.2007.02.059.
[40] G. De Nisco, A. Hoogendoorn, C. Chiastra, et al., The impact of helical flow on coronary atherosclerotic plaque development, Atherosclerosis 300 (2020) 39–46, https://doi.org/10.1016/j.atherosclerosis.2020.01.027.
[41] E.C. Viel, C.A. Lemarie, K. Benkirane, et al., Immune regulation and vascular inflammation in genetic hypertension, Am. J. Physiol. Heart. Circ. Physiol. 298 (2010) 938–944, https://doi.org/10.1152/ajpheart.00707.2009.
[42] K. Hirata, T. Ishida, H. Matsushita, et al., Regulated expression of endothelial cellderived lipase, Biochem. Biophys. Res. Commun. 272 (2000) 90–93, https://doi.org/10.1006/bbrc.2000.2747.
[43] T. Korff, K. Aufgebauer, M. Hecker, Cyclic stretch controls the expression of cd40 in endothelial cells by changing their transforming growth factor-beta 1 response, Circulation 116 (2007) 2288–2297, https://doi.org/10.1161/circulationaha.107.730309.
[44] H. Zhao, T. Hiroi, B.S. Hansen, et al., Cyclic stretch induces cyclooxygenase-2 gene expression in vascular endothelial cells via activation of nuclear factor kappa-beta, Biochem. Biophys. Res. Commun. 389 (2009) 599–601, https://doi.org/10.1016/j.bbrc.2009.09.028.
[45] M. Watase, M.A. Awolesi, J. Ricotta, et al., Effect of pressure on cultured smooth muscle cells, Life Sci. 61 (1997) 987–996, https://doi.org/10.1016/s0024-3205(97)00603-6.
[46] A. Tziotziou, E.M.J. Hartman, S.A. Korteland, et al., Mechanical wall stress and wall shear stress are associated with atherosclerosis development in non-calcified coronary segments, Atherosclerosis 387 (2023) 117387, https://doi.org/10.1016/j.atherosclerosis.2023.117387.
[47] N. Bergh, P. Larsson, E. Ulfhammer, et al., Effect of shear stress, statins and TNF-α on hemostatic genes in human endothelial cells, Biochem. Biophys. Res. Commun. 420 (1) (2012) 166–171, https://doi.org/10.1016/j.bbrc.2012.02.136.
[48] S.Z. Gu, C. Costopoulos, Y. Huang, et al., High-intensity statin treatment is associated with reduced plaque structural stress and remodelling of artery geometry and plaque architecture, Eur. Heart. J. Open. 1 (3) (2021) 39, https://doi.org/10.1093/ehjopen/oeab039.
[49] R. Torii, J. Keegan, N.B. Wood, et al., MR image-based geometric and hemodynamic investigation of the right coronary artery with dynamic vessel motion, Ann. Biomed. Eng. 38 (2010) 2606–2620, https://doi.org/10.1007/s10439-010-0008-4.